Oceanic Warming Has Lengthened Intense Tropical Cyclone Seasons Globally

Jeremy Leung

chleung@pku.edu.cn

College of Meteorology and Oceanography, National University of Defense Technology
https://orcid.org/0000-0002-4325-1083

Jimmy Liu

College of Atmospheric Sciences, Lanzhou University

Dingchi Zhao

College of Meteorology and Oceanography, National University of Defense Technology

Daosheng Xu

Guangzhou Institute of Tropical and Marine Meteorology/Guangdong Provincial Key Laboratory of Regional Numerical Weather Prediction, China Meteorological Administration

Hong Huang

College of Meteorology and Oceanography, National University of Defense Technology

Zengliang Zang

College of Meteorology and Oceanography, National University of Defense Technology

Wenshou Tian

Lanzhou University https://orcid.org/0000-0002-4700-4194

Yaoming Ma

Institute of Tibetan Plateau Research, Chinese Academy of Sciences

Yi Li

College of Meteorology and Oceanography, National University of Defense Technology

Banglin Zhang

College of Meteorology and Oceanography, National University of Defense Technology

Physical Sciences - Article

Keywords:

Posted Date: January 30th, 2025

DOI: https://doi.org/10.21203/rs.3.rs-5838052/v1

Additional Declarations: There is **NO** Competing Interest.

Oceanic Warming Has Lengthened Intense Tropical Cyclone Seasons Globally

Jimin Liu[1,2,3,4#], Jeremy Cheuk-Hin Leung[1#], Dingchi Zhao[1], Daosheng Xu[5], Hong Huang[1], Zengliang Zang[1], Wenshou Tian[4], Yaoming Ma[3,4,6,7,8], Yi Li[1*], Banglin Zhang[1,4*]

Affiliations

[1] College of Meteorology and Oceanography, National University of Defense Technology, Changsha, China

[2] Northwest Institute of Eco-Environment and Resources, Chinese Academy of Sciences, Lanzhou, China

[3] University of Chinese Academy of Sciences, Beijing, China

[4] College of Atmospheric Sciences, Lanzhou University, Lanzhou, China

[5] Guangzhou Institute of Tropical and Marine Meteorology / Guangdong Provincial Key Laboratory of Regional Numerical Weather Prediction, CMA, Guangzhou, China

[6] Land-Atmosphere Interaction and Its Climatic Effects Group, State Key Laboratory of Tibetan Plateau Earth System, Environment and Resources, Institute of Tibetan Plateau Research, Chinese Academy of Sciences, Beijing, China

[7] Key Laboratory of Land Surface Process and Climate Change in Cold and Arid Regions, Northwest Institute of Eco-Environment and Resources, Chinese Academy of Sciences, Lanzhou , China

[8] Kathmandu Center of Research and Education, Chinese Academy of Sciences, Beijing, China

# These authors contributed equally to this work

* Correspondence to: zhangbanglin24@nudt.edu.cn (Banglin Zhang), liyiqxxy@163.com (Yi Li)

Abstract

Intense tropical cyclones (TCs), which pose significant threats to human life and property, often occur within a short period of time each year, known as the intense TC season. Changes in the lengths of intense TC seasons under climate change are critical scientific and socioeconomic issues. While recent research has investigated trends in overall TC seasons, the response of intense TC seasons to climate change remains underexplored. Here, we discover that intense TC seasons have been lengthening globally since 1980, with significant increasing trends ranging from 8.5–14.2 days/decade across all basins, equivalent to 6.5-21.2% increase in intense TC season lengths per decade. This is primarily driven by the enhancing thermodynamic disequilibrium between ocean and atmosphere due to recent oceanic warming, which raises the maximum potential intensity of TCs outside the traditional intense TC seasons. Meanwhile, changes in atmospheric circulation play a minor role. As a result, off-season TCs are more likely to develop into intense TCs. The findings in this study indicate an increasing exposure of human societies to intense TC risks outside historical seasonal norms. This suggests the urgent need for preparation and mitigation measures for the potential risks of intense TCs under future climate change.

Main Text

Intense tropical cyclones (TCs), or Category 4–5 storms that have lifetime maximum intensities (LMI) exceeding 113 knots, are responsible for the majority of TC-related disasters each year, causing extensive damage and loss of life due to their strong winds, heavy rainfall, and storm surges [1–3]. These intense TCs require substantial potential energy from the atmosphere and ocean, typically occurring during a relatively short period, known as the intense TC season. Despite their infrequent occurrence, the consequences of intense TCs for human society and the environment are significant. For instance, in 2024, the recent record-breaking Hurricane Beryl in the North Atlantic (NA) and Cyclone Chido in the South Indian Ocean (SI) caused substantial destruction [4,5]. Given the huge impact of intense TCs, it is crucial to study how climate change may influence their activity [1,6,7].

Over the past decades, anthropogenic warming has significantly altered the seasonal cycle of the climate system. Research indicates that the length of summer has been extended, whereas winter has shortened, owing to the altered timing of seasonal transitions under greenhouse warming [8–10]. Furthermore, the seasonality of sea surface temperature (SST) and oceanic warm pool has also been affected [11,12]. Notably, anthropogenic forcing has been found to enhance the amplitude of the global SST seasonal cycle by $3.9 \pm 1.6\%$ from 1983–2022 [13]. These changes in Earth's seasonal cycle are hypothesized to influence the activity of weather systems and extreme events that are seasonally dependent [14–18]. In particular, the shift in the seasonal distribution of atmospheric and oceanic conditions favorable for TC development may modulate the likelihood of TCs occurring during specific months and seasons, hence influencing the behavior of TC seasons.

The above hypothesis is evident in numerous studies [19,20], especially those documenting the effects of climate change on the onset and withdrawal timing [21–25], as well as the lengths [20,26–28] of overall TC seasons (see Methods for definitions). However, long-term changes in intense TC activities may differ from those of overall TC seasons because of their different evolution patterns and controlling factors, especially the substantial energy required for the development of intense TCs. Research has reported that anthropogenic forcings have resulted in atmospheric and oceanic environments more favorable to TC rapid intensification, which has consequently led to a higher occurrence of intense TCs globally over the past four decades [29–33]. Climate simulations also indicate a significant increase in the frequency of intense TCs over much of the global ocean [34–36]. In particular, a recent study has identified a shift in the peak occurrence of global intense TCs from autumn to summer and attributed it to the seasonal heterogeneity of oceanic warming [37].

Given the profound risks associated with intense TC disasters, even minor changes in the timing of intense TC seasons can have substantial consequences. However, to date, while plenty of works have discussed the impacts of climate change on the seasonality of TC activity, very few have put their focus on that of intense TCs [37]. It remains unclear to what extent the altering atmospheric

and oceanic seasonal cycles have influenced the lengths of intense TC seasons under past anthropogenic warming.

In this paper, we thoroughly address this particular issue by estimating changes in intense TC seasons over the NA, eastern North Pacific (ENP), western North Pacific (WNP), SI, and South Pacific (SP) basins, as well as quantitively examining the main underlying drivers. Our results indicate significant lengthening trends of intense TC seasons globally, despite the relatively stable overall TC seasons. This is primarily attributed to the increased efficiency of off-season TCs developing into intense TCs, driven by the enhancing environmental maximum potential intensity (MPI) induced by oceanic warming. The findings imply that intense TCs have become more common during periods traditionally considered off-season, potentially leading to a higher risk of intense TC-related disasters and associated societal and economic consequences.

Results

Lengthening Intense TC Seasons

Intense TC seasons, defined as the period in which 90% of intense TCs occur in a year (see Methods), typically last for a short period, covering 34–82% of the overall TC seasons. Climatologically, the globally average intense TC season length is 96.3 days, with the shortest observed in the NA (42.2 days) and the longest in the WNP (172.7 days). For most basins, the intense TC seasons generally occur in late summer and early autumn (Supplementary Text S1, Figs. S1–S2, Table S1), when the ocean and atmosphere accumulate sufficient potential energy to allow a TC to intensify to a Category 4–5 storms.

As the seasonality of the climate system changes under global warming [8,12,13], the climatology of intense TC seasons is also affected. Based on historical TC observations, we find that the durations of intense seasons have increased significantly for both hemispheres and all basins since 1980. Specifically, from 1980–2023, the intense TC seasons in the Northern Hemisphere (NH) and Southern Hemisphere (SH) significantly lengthened by 6.3 (Figs. 1a,1d) and 9.1 (Figs. 1b,1e) days/decade, respectively. For specific basins, in the NH, the lengths of intense TC seasons in the NA, ENP, and WNP increased by 8.9 (Fig. 1f), 10.9 (Fig. 1g), and 11.2 (Fig. 1h) days/decade, respectively. Meanwhile, in the SH, the intense TC season lengths in the SI and SP increased by 8.5 (Fig. 1i) and 14.2 (Fig. 1j) days/decade, respectively.

We further find that the lengthening patterns of intense TC seasons are basin-dependent (Fig. 1c). Three types of lengthening patterns are recognized. (1) The first type of lengthening (TYPE I) is characterized by an earlier start of the intense TC season, but without significant change in the season end date. The lengthening trends of SI, SP, and ENP intense TC seasons belong to TYPE I (Figs. 2c, 2g, 2i). (2) TYPE II lengthening is also primarily due to an earlier start of the intense TC season, but is partly offset by the earlier shift of the end of the season. The lengthening intense TC

season in the WNP belongs to TYPE II (Fig. 2e). (3) TYPE III lengthening, in contrast, is characterized by a later end of intense TC season. The lengthening NA intense TC season belongs to this type (Fig. 2a). This suggests the complexity of the changes in the intense TC seasons across different basins (Supplementary Text S2, Fig. S3, Table S2).

The above results indicate that the intense TC seasons have become 1–2 weeks longer every 10 years, equivalent to a relative change of 6.5–21.2%/decade. These lengthening trends of intense TC seasons are insensitive to the definitions of intense TC seasons (Fig. 2, Supplementary Fig. S4 and Table S3), confirming the robustness of the above conclusions (Supplementary Text S3).

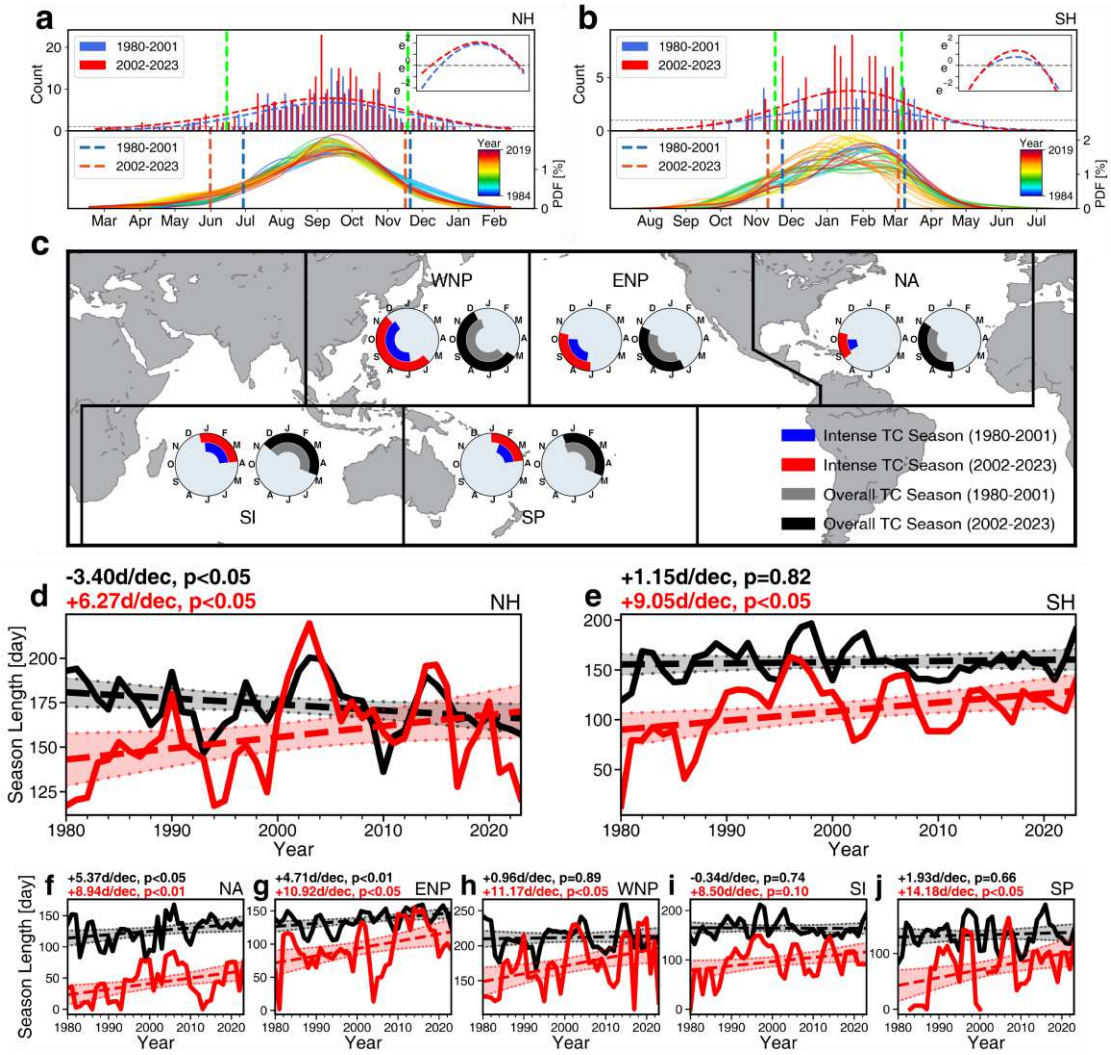

Fig. 1 | Lengthening trends of intense TC seasons from 1980–2023. a–b, Upper panel: Statistical distributions of intense TC occurrence (bars, 5 days interval) during 1980–2001 (blue) and 2002–2023 (red) in the NH **(a)** and SH **(b)**, where the dashed curves represent the Gaussian fit curves. The top-right panel is the same, except with a log-scale y-axis. Lower panel: Similar to the upper panel, but the Gaussian fitting is applied to data for every 9 years. The green, blue, and red vertical dashed lines denote the average start and end dates of the intense TC seasons during 1980–2023, 1980–2001, and 2002–2023, respectively. **c,** Temporal coverage of intense TC seasons (blue for 1980–2001, red for 2002–2023) and overall TC seasons (grey for 1980–2001, black for 2002–2023) over

the five basins. **d–j,** Lengths (unit: day) of intense TC seasons (red) and overall TC seasons (black) over the NH **(d)**, SH **(e)**, NA **(f)**, ENP **(g)**, WNP **(h)**, SI **(i)**, SP **(j)**, respectively. Dashed lines denote the linear trends of time series. Shading denotes the 95% confidence interval. Results are based on intense TC records in the IBTrACS from 1980–2023. Results show that the intense TC season lengths of all basins have been increasing significantly from 1980–2023.

Off-season storms are more likely to develop into intense TCs

The increasing trends in the lengths of intense TC seasons imply a higher probability of intense TCs occurring outside of traditional intense TC seasons. However, it is important to note that the number of TC genesis (*TCG*) does not necessarily increase during the pre-season and post-season periods [25,38,39]. This is reflected in the inconsistent lengthening trends between intense TC season and overall TC seasons (Fig. 1c), of which the latter is defined as the period when the majority of TCs occur (see Methods). Using the same dataset and study period, we find that the trends in overall TC season lengths across the WNP, SI, and SP are statistically insignificant (Figs. 1h–1j). Meanwhile, although significant lengthening trends are observed in the overall TC seasons over the NA (+5.4 days/decade; Fig. 1f) and ENP (+4.7 days/decade; Fig. 1g), these trends are much smaller in magnitudes compared to those for intense TC seasons. As a whole, we observe a reduction in the NH overall TC season length (-3.4 days/decade; Fig. 1d) and no significant change in the SH. These observations contrast with the significant increase in intense TC season lengths, suggesting that changes in off-season TCG may not be the main reason driving the lengthening of intense TC seasons (Supplementary Text S4).

Instead, we find that the efficiency of TCs developing into intense TCs (α), which indicates how likely a TC reaches Category 4–5, is the primary factor contributing to the lengthening of intense TC seasons. By decomposing the trends in pre-season and post-season intense TC numbers ($\Delta N/\Delta t$) into changes in α ($\Delta\alpha/\Delta t$) and *TCG* ($\Delta TCG/\Delta t$), we can quantify to what extent $\Delta\alpha/\Delta t$ and $\Delta TCG/\Delta t$ respectively contribute to the trends in intense TC season lengths (Eq. 2). For instance, for TYPE I basins (ENP, SI, SP) which are featured with earlier starts of intense TC season, we find that the rise in pre-season *N* is almost entirely attributed to the increase in α. In comparison, $\Delta TCG/\Delta t$ contributes negligibly to the increase in pre-season *N* over the ENP and SI, while the SP even exhibits a decrease in pre-season *TCG*, offsetting the α increasing trend. Similarly, the earlier start of intense TC season in TYPE II basin (WNP) is also predominantly due to the increase in pre-season α, accounting for 99.8%. For Type III basins (NA), where the lengthening intense TC season is due to a later end of the season, $\Delta\alpha/\Delta t$ and $\Delta TCG/\Delta t$ account for 74.2% and 40.4% of the increase in post-season *N*, respectively (Fig. 2k, Supplementary Text S5).

The above results suggest that, under the past climate change, TCs are more likely to intensify and become intense TCs during pre-season (for WNP, ENP, SI, and SP) and post-season (for NA) periods. This is the primary reason leading to the lengthening of intense TC seasons over all basins. No matter for which lengthening type, changes in the number of TCG play a minor role.

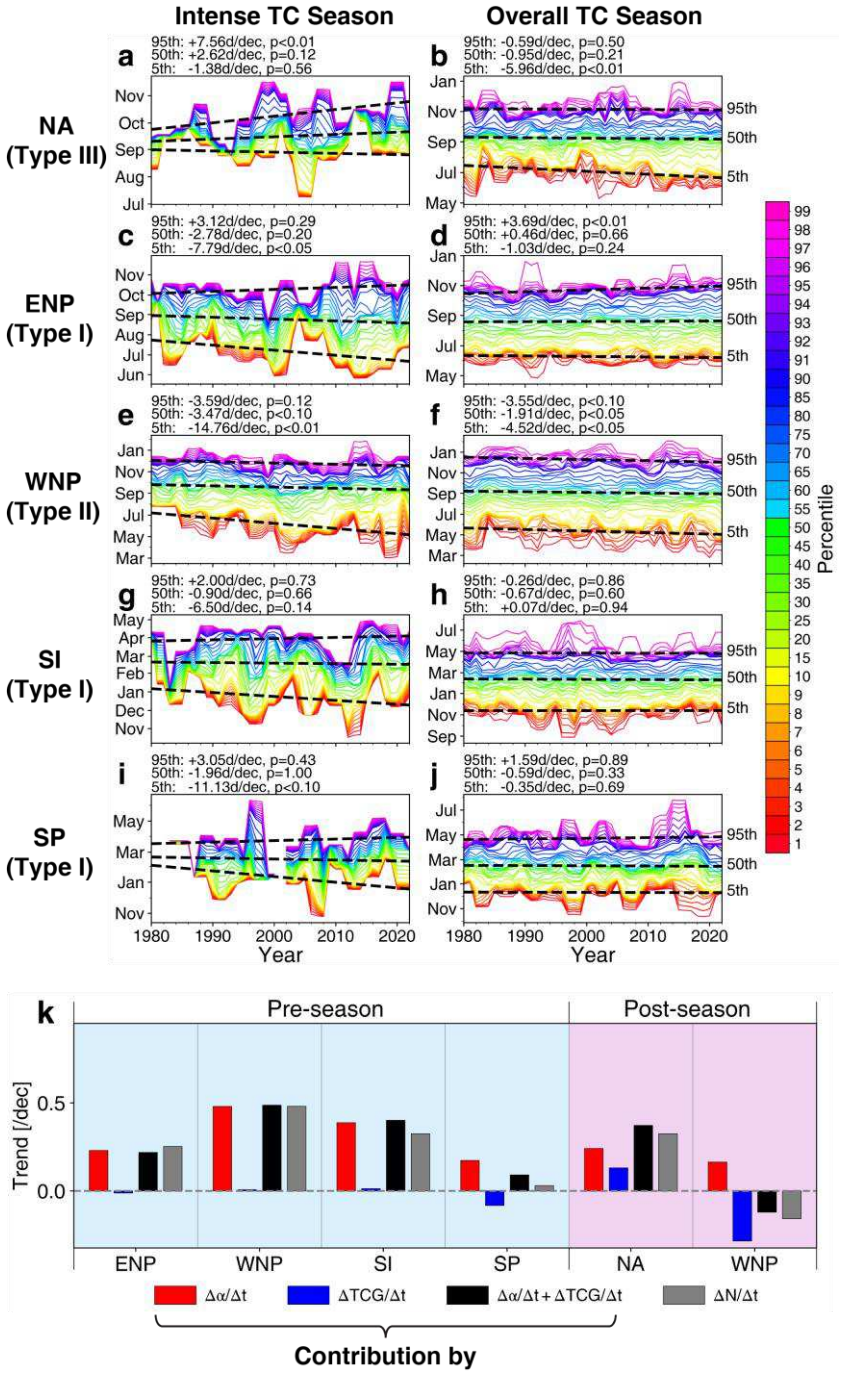

Fig. 2 | Contributions of changes in α and *TCG* to the lengthening of intense TC seasons. a, Annual time series of different percentiles of occurrence time of intense TCs over the NA, with smaller percentiles referring to TCs that occur earlier in a year. **b,** Same as **(a)**, except for all TCs with LMI greater than 34 knots. **c–j,** Same as **(a–b)**, except for the ENP **(c–d)**, WNP **(e–f)**, SI **(g–h)**, and SP **(i–j)**, respectively. The three black dashed lines denote the linear trends of the 5th (start date), 50th (median), and 95th (end date) percentiles, respectively. Shadings denote the 95% confidence interval. **k,** Trends in intense TC number ($\Delta N/\Delta t$, Eq. 1, grey, unit: decade^{-1}), as well as the contributions of changes in α ($\overline{TCG} \times \Delta\alpha/\Delta t$, Eq. 2, red, unit: decade^{-1}), *TCG* ($\bar{\alpha} \times \Delta TCG/\Delta t$, Eq. 2, blue, unit: decade^{-1}), and their sum ($\overline{TCG} \times \frac{\Delta\alpha}{\Delta t} + \bar{\alpha} \times \Delta TCG/\Delta t$, Eq. 2, black, unit: decade^{-1}). Results are based on the IBTrACS from 1980–2023. Results show that the lengthening trends of intense TC seasons are primarily attributed to the increasing likelihood that off-season TCs develop into intense TCs, i.e., $\Delta\alpha/\Delta t$.

Minor roles of changes in TCG and environmental atmospheric circulation

Despite its negligible contributions to the off-season $\Delta N/\Delta t$ in the ENP, SI, and SP, $\Delta TCG/\Delta t$ acts as a minor factor influencing the lengths of intense TC season in the WNP and NA. In the NA, the increasing number of TCG accounts for 40.4% of the delay in the end of intense TC season (Fig. 2k). This post-season TCG trend, which is well indicated by the dynamic genesis potential index [40,41] (DGPI, see Methods), is primarily attributed to a significant reduction in vertical wind shear (V_{shear}) over the NA domain, accounting for 67.9% (Figs. 3a, 3c). This weakening V_{shear} is associated with the slowdown in upper-tropospheric circulation of the region [42] (Supplementary Text S6 and Fig. S5). In contrast, other factors exhibit insignificant changes (Figs. 3e, 3g, 3i).

In the WNP, the negative $\Delta TCG/\Delta t$ leads to an earlier shift of the end of intense TC season, which partially offsets the lengthening trend caused by pre-season $\Delta\alpha/\Delta t$ (Fig. 2k). In this case, the enhancing background large-scale downdrafts and V_{shear} are the major causes of the decrease in post-season TCG, which contributes 49.0% and 42.8%, respectively (Figs. 3b, 3d, 3h). While the former is a result of the response of Walker circulation to global warming [43,44], the latter may be associated with interdecadal variability of monsoon transition and AMO [38,45] (Supplementary Text S7 and Fig. S6).

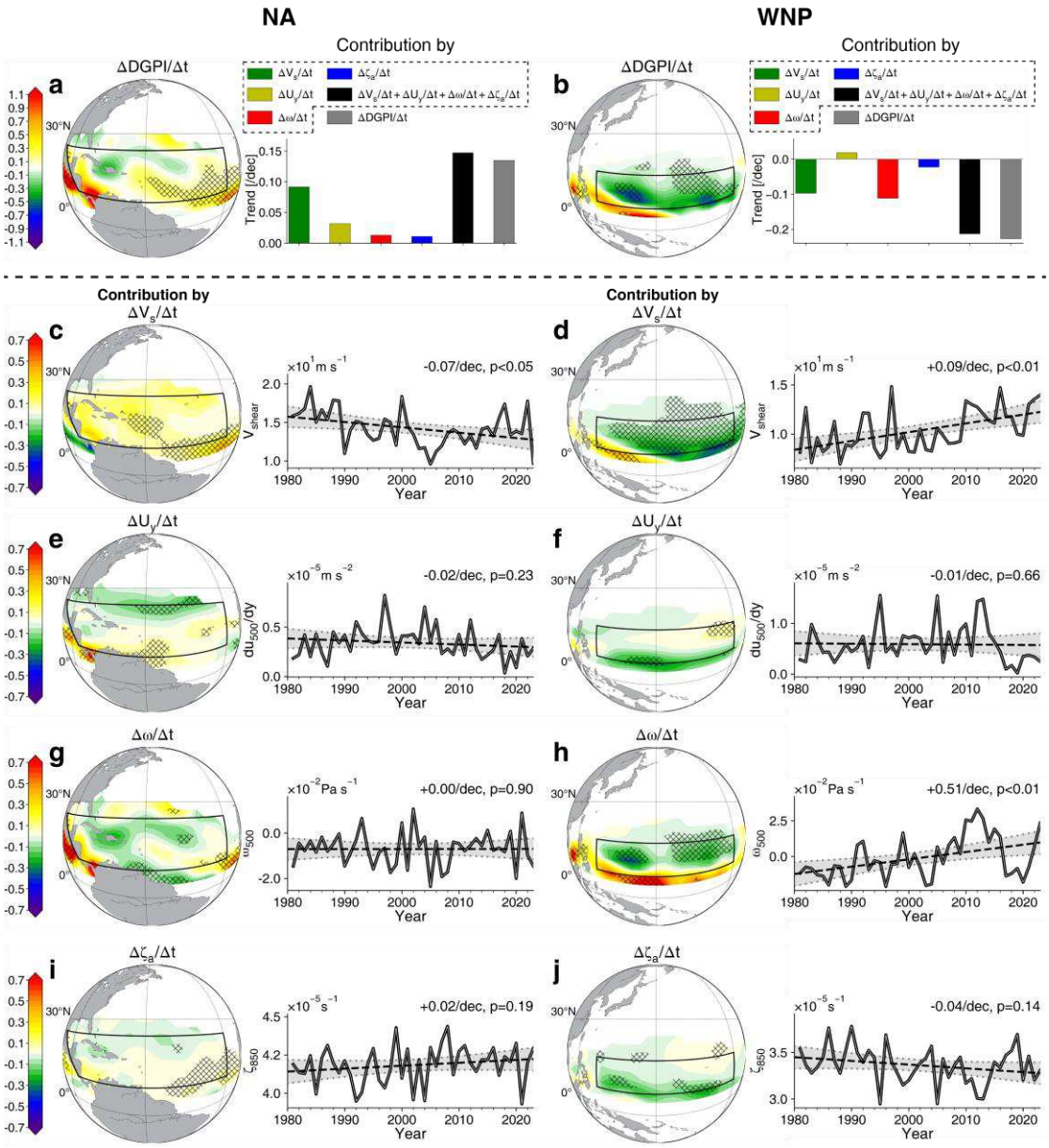

Fig. 3 | Factors driving the increase in DGPI and TCG. a–b, Spatial distribution of post-season DGPI trends ($\Delta DGPI/\Delta t$, Eq. 4, unit: deacde^{-1}) from 1980–2023 (left panels) over the NA **(a)** and WNP **(b)**, with black boxes denoting the key areas where intense TCs formed and intensified (Supplementary Fig. S1). The meshed areas denoting significant trends at the 95% confidence level. The right panels plot the domain-mean $\Delta DGPI/\Delta t$ (grey, unit: deacde^{-1}), as well as the contributions of $\Delta V_s/\Delta t$ (green, unit: deacde^{-1}), $\Delta U_y/\Delta t$ (yellow, unit: deacde^{-1}), $\Delta\omega/\Delta t$ (red, unit: deacde^{-1}), $\Delta\xi_a/\Delta t$ (blue, unit: deacde^{-1}), and their sums (black, unit: deacde^{-1}) (Eq. 5). **c–d,** Same as **(a–b)**, except for spatial distribution of contributions of $\Delta V_s/\Delta t$ (left, unit: deacde^{-1}) and time series of domain-mean V_{shear} (right, unit: m s^{-1}). **e–f,** Same as **(c–d)**, except for spatial distribution of contributions of $\Delta U_y/\Delta t$ (left, unit: deacde^{-1}) and time series of domain-mean $\frac{du_{500}}{dy}$ (right, unit: m s^{-2}). **g–h,** Same as **(c–d)**, except for spatial distribution of contributions of $\Delta\omega/\Delta t$ (left, unit: deacde^{-1}) and time series of domain-mean ω_{500} (right, unit: Pa s^{-1}). **i–j,** Same as **(c–d)**, except for spatial distribution of contributions of $\Delta\xi_a/\Delta t$ (left, unit: deacde^{-1}) and time series of domain-mean ξ_{850} (right, unit: s^{-1}). Grey shading denotes the 95% confidence interval. Results show that the later end of NA intense TC season is caused by the weakening

environmental V_{shear}; meanwhile, the earlier end of WNP intense TC season is the combined result of the weakening V_{shear} and strengthening background downdraft circulation.

Major roles of $\Delta\alpha/\Delta t$ and oceanic warming

As mentioned earlier, no matter for which basins, the lengthening trends of intense TC seasons are primarily attributed to the increase in off-season α. Namely, a growing proportion of TCs have been intensifying to Category 4–5 during pre-season periods for the ENP, WNP, SI, and SP, as well as post-season for the NA. A key question is, what is the underlying mechanism that favors off-season storms developing into intense TCs more easily?

The likelihood of a TC developing into an intense TC is closely related to its MPI [30,31] (see Methods). Results show significant increasing trends in the average pre-season MPI over the ENP (1.55 m s^{-1} $decade^{-1}$), WNP (2.60 m s^{-1} $decade^{-1}$), SI (1.83 m s^{-1} $decade^{-1}$), and SP (2.67 m s^{-1} $decade^{-1}$), as well as the post-season MPI over the NA (+1.87 m s^{-1} $decade^{-1}$) from 1980–2023. These are consistent with the above-mentioned trends in the off-season $\overline{TCG} \times \frac{\Delta\alpha}{\Delta t}$. MPI can be decomposed into the thermodynamic efficiency term (η) and the thermodynamic disequilibrium between the sea surface and troposphere (L) of the TC's surrounding environment. While the former is more sensitive to upper tropospheric temperature, the latter is generally governed by the SST variability [46–48]. To investigate the cause of increasing off-season α, which leads to the lengthening of global intense TC seasons, we quantitatively estimate the contributions of changes in η ($\Delta\eta/\Delta t$) and L ($\Delta L/\Delta t$) to trends in MPI ($\Delta MPI/\Delta t$) (see Methods).

Results show that the increasing MPIs of off-season storms are predominantly driven by the enhancing background thermodynamic disequilibrium (Fig. 4a). In Type I basins, where the pre-season $\Delta\alpha/\Delta t$ is responsible for the lengthening of intense TC seasons, changes in L contribute to pre-season $\Delta MPI/\Delta t$ basins by 75.4% for the ENP (Figs. 4b–4e), 67.7% for the SI (Figs. 4j–4m), and 86.8% for the SP (Figs. 4n–4q), respectively. In the WNP (TYPE II), where the lengthening intense TC season is also attributed to the increase in pre-season α, $\Delta L/\Delta t$ accounts for 85.5% of the pre-season *MPI* increase (Figs. 4f–4i). For the NA (TYPE III), where the post-season $\Delta\alpha/\Delta t$ explains the extension of intense TC season duration, 66.3% of the post-season $\Delta MPI/\Delta t$ is contributed by ($\Delta L/\Delta t$) (Figs. 4r–4u). On the contrary, the increasing η has limited effects on the rising trends of MPI, with contributions ranging from 13.1–33.1% (Fig. 4a) (Supplementary Text S8).

These findings suggest that the thermodynamic disequilibrium term plays a primary role in causing more off-season TCs to develop into intense TCs, thereby increasing the off-season MPI and extending the duration of intense TC seasons. Although various types of lengthening are observed, our results indicate that $\Delta L/\Delta t$ is the key factor determining the changes in lengths of intense TC seasons, independent of basin or lengthening types. This aligns with previous studies that identified L as the main driver of *MPI* seasonality [46]. Since L is typically controlled by the sea

surface temperature [46,48], it is the warming sea surface that amplifies the gradient of saturation moist static energy between the sea surface and the free troposphere, which then leads to the lengthening of intense TC seasons under climate change.

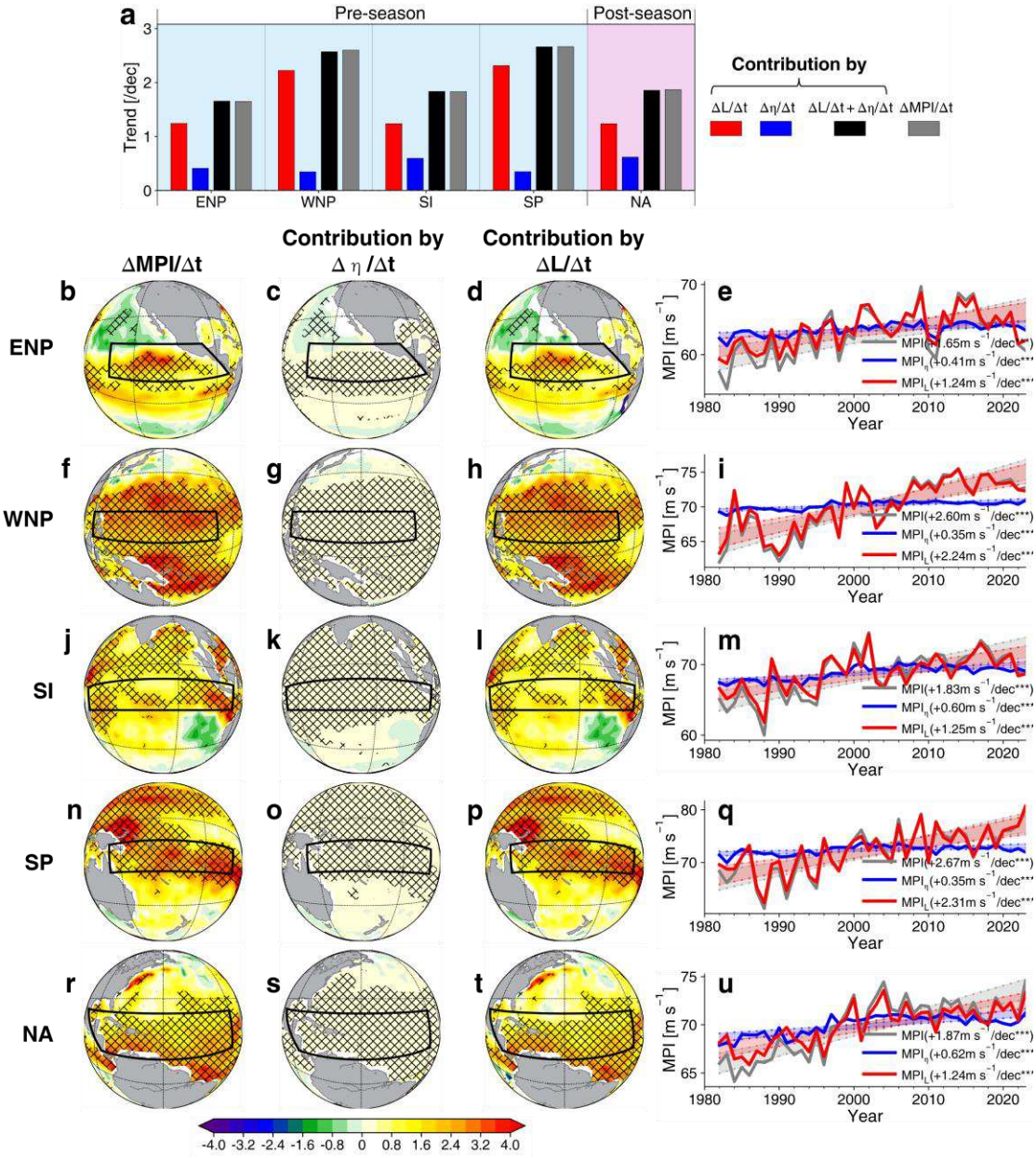

Fig. 4 | The role of thermal disequilibrium term in increasing MPI and α. a, the domain-mean $\Delta MPI/\Delta t$ (grey, unit: m s^{-1} deacde^{-1}), as well as the contributions of $\Delta L/\Delta t$ (blue, unit: m s^{-1} deacde^{-1}), $\Delta \eta/\Delta t$ (red, unit: m s^{-1} deacde^{-1}), and their sums (black, unit: m s^{-1} deacde^{-1}) (Eq. 7). **b–d,** Spatial distribution of pre-season $\Delta MPI/\Delta t$ **(b)**, as well as those of contributions by $\Delta L/\Delta t$ **(c)**, $\Delta \eta/\Delta t$ **(d)**, from 1980–2023 over the ENP. The meshed areas denote significant trends at the 95% confidence level. The black boxes denote the key areas where intense TCs formed and intensified (Supplementary Fig. S1). **e,** Annual-mean series (unit: m s^{-1}) of the domain-mean MPI (black), MPI_L (blue, Eq. 8), and MPI_η (red, Eq. 9) over the ENP, where the latter two indicate MPI variability caused by $\Delta L/\Delta t$ and $\Delta \eta/\Delta t$, respectively (Eq. 8). Shadings denote the 95% confidence interval. **f–u,** Same as **(b–e)**, but for pre-season WNP **(f–i)**, pre-season SI **(j–m)**, pre-season SP **(n–q)**, and post-season NA **(r–u)**,

respectively. Results show that the thermal disequilibrium term (*L*) plays the dominant role in increasing the likelihood that a TC develops into an intense TC, hence leading to the global lengthening of intense TC seasons.

Discussion

The lengths of intense TC seasons directly influence the number of days human society is exposed to the potential threat of Category 4–5 storms. In this study, we discover that, since 1980, the lengths of intense TC seasons have been extending across all basins, with significant trends ranging from 8.5–14.2 days/decade. This corresponds to 6.5-21.2% increase in intense TC season lengths per decade. The lengthening trends are mainly characterized by an early onset of season (for the ENP, WNP, SI, and SP), whereas the NA exhibits a late withdrawal of season.

Analyses indicate that oceanic warming is the primary driver for this trend, as it enhances the thermodynamic disequilibrium between the sea surface and the troposphere, thereby increasing the likelihood of off-season TCs developing into intense TCs. This conclusion aligns with previous research indicating that oceanic warming leads to an earlier shift in TC activity[22,28,37]. While previous studies claimed that rapid intensification contributes to the variability in intense TC activity, further analyses will be needed to examine its roles in the observed lengthening of intense TC seasons.

While the response of overall TC seasons to climate change may vary and even contrast across basins [25,38,39], our findings indicate a consistent lengthening of intense TC seasons on a global scale due to past anthropogenic warming. This suggests a higher probability of intense TC disasters occurring outside traditional intense TC seasons. The more frequent off-season intense TCs further imply a greater chance of human society facing compound extreme weather events resulting from the intersection of intense TCs with other weather systems during off-seasons, such as winter extratropical cyclones. This could lead to more extreme rainfall and flooding, resulting in more severe infrastructure damage and heightened risks to public safety during periods traditionally considered safe from intense TC threats [37,49,50]. Therefore, this study emphasizes the urgent need to reevaluate and strengthen disaster resilience and recovery strategies and risk mitigation efforts to address the increasing risks associated with these rarely occurring weather patterns under future climate scenarios.

Methods

Data

All TC data utilized in this study were obtained from version 4 of the International Best Track Archive for Climate Stewardship (IBTrACS v4r01) [51]. The IBTrACS collects historical TC observation records from official meteorological agencies, which provides more reliable data sources of intense TCs than other available datasets [52]. It is noted that the standards of measurement vary across regions. In this study, for TCs over all basins, we use the 10-minute maximum sustained wind speed records reported by the National Oceanic and Atmospheric Administration (NOAA) ($Wind_{USA}$), to ensure a consistent global standard.

The SST data analyzed in this study were provided by the NOAA High-resolution Blended Analysis of Daily SST (OISSTv2) with a 0.25°x0.25° grid [53]. The data of atmospheric variables analyzed were obtained from the NOAA NCEP/DOE Reanalysis 2 (NCEP2) [54], which provides data of vertical velocity, u and v components of horizontal wind speed, and air temperature, with a horizontal resolution of 2.5° × 2.5°. Note that because the OISSTv2 only provides data since September 1981, the analyses in this study that involved these data were limited to the period of 1982–2023. Nevertheless, this does not affect the conclusions of this study.

Identification of intense TCs

In this study, a TC is defined if its LMI is larger than 34 knots. And, a TC is considered intense when its LMI exceeds 113 knots, which is equivalent to Category 4–5 hurricanes in the Saffir-Simpson Hurricane Wind Scale. The occurrence time of a TC is taken as the time when the TC first reaches its LMI. As in previous studies[37,52], only intense TCs in the NA, EP, WP, SI, and SP were analyzed in the study.

Start and end dates of intense TC seasons and overall TC seasons

The start and end dates of intense TC seasons and overall TC seasons are estimated for each hemisphere and each basin based on the TC occurrence time[20,55], based on the IBTrACS data at 00/06/12/18 UTC. In our calculations, we first determine the occurrence time of each detected intense TC, which is defined as the first time when the TC reaches its LMI. Then, for each year, the start and end dates are defined as the 5^{th} and 95^{th} percentile values of the intense TC occurrence time within a 3-year period. The use of 3-year data points helps reduce uncertainties caused by the small number of intense TC cases each year [29]. Note that because of the opposite seasonal cycle between the NH and SH, we set a year of the NH and SH beginning on 16 February and 16 August, respectively. Following the same procedure, the start and end dates of the overall TC season are defined as the 5th and 95th percentiles of the occurrence time of all TCs with LMI greater than 34 knots within a 3-year window.

In the main text, in order to explain variations in the lengths of intense TC seasons, we analyze changes in TC activity during the pre-season and post-season periods. Technically, the pre-season period for a basin is defined as the 30-day period prior to the start date of the intense TC season for that basin. Similarly, the post-season period is defined as the 30-day period following the end date of the intense TC season.

It is noted that different percentile values have been used to define TC seasons[20,23]. Although some studies may adopt stricter definitions, the definition employed in this study is the least sensitive to outlier data points, which ensures more reliable and robust results in the time series analysis of intense TC season lengths. Additional analyses have confirmed that the conclusions of this study are not affected by the choice of definitions (more details in Supplementary Text S3).

Efficiency of a TC developing into an intense TC

Changes in intense TC season duration can be regarded as changes in intense TC numbers over the pre-season and post-season periods. The number of intense TCs (*N*) is determined by the number of TCs formed (i.e., *TCG*) and the proportion of TCs that develop into intense TCs (*α*). Mathematically, this can be simply expressed as:

$$N = TCG \times \alpha \qquad (1)$$

According to Eq. 1, changes in either *TCG* or *α* can affect *N*, and hence lead to changes in the length of intense TC season. In particular, *α* indicates how likely a TC will develop into an intense TC. In this study, in order to examine the reason for the lengthening of intense TC season, we quantitatively estimate the contribution of changes in *TCG* or *α* to that in *N*, respectively. This can be simply done by the product rule of calculus:

$$\frac{\Delta N}{\Delta t} \approx \overline{TCG} \times \frac{\Delta \alpha}{\Delta t} + \bar{\alpha} \times \frac{\Delta TCG}{\Delta t} \qquad (2)$$

where the operator $\frac{\Delta}{\Delta t}$ denotes the long-term linear trend, and the bar denotes the long-term average. On the right-hand side of Eq. (2), the first term ($\overline{TCG} \times \frac{\Delta \alpha}{\Delta t}$) indicates the contribution of changes in *α* to that in *N*. Similarly, the second term ($\bar{\alpha} \times \frac{\Delta TCG}{\Delta t}$) indicates the contribution of changes in *TCG*. By comparing the signs and magnitudes of the two terms, one can quantitatively identify the major factor affecting the intense TC season length of each basin.

Dynamical genesis potential index

The dynamical genesis potential index (*DGPI*), which can better capture the long-term variability of TCG [40,41], was used to analyze the changes in post-season TCGs in the WNP and NA. According to previous studies, the DGPI can be expressed as a combination of four factors [40,41]:

$$DGPI = V_s \times U_y \times \omega \times \zeta_a \times e^{-11.8} - 1.0 \qquad (3)$$

$$DGPI = (2.0 + 0.1 \times V_{shear})^{-1.7} \left(5.5 - 10^5 \times \frac{du_{500}}{dy}\right)^{2.3} (5.0 - 20 \times \omega_{500})^{3.4} (5.5 + |10^5 \times \zeta_{850}|)^{2.4} e^{-11.8} - 1.0 \qquad (4)$$

where $V_s = (2.0 + 0.1 \times V_{shear})^{-1.7}$ denotes the vertical wind shear (V_{shear}) term, $U_y = \left(5.5 - 10^5 \times \frac{du_{500}}{dy}\right)^{2.3}$ denotes the meridional gradient of 500-hPa zonal wind ($\frac{du_{500}}{dy}$) term, $\omega = (5.0 - 20 \times \omega_{500})^{3.4}$ denotes the 500-hPa vertical wind (ω_{500}) term, $\zeta_a = (5.5 + |10^5 \times \zeta_{850}|)^{2.4}$ denotes the 850-hPa absolute vorticity (ζ_{850}) term, respectively.

In order to quantify the contribution of the change in each term in Eq. (4) to that in *MPI*, we follow the same decomposition method as in Eq. (2), and apply the product rule to the first derivative of Eq. (4). Hence, the long-term trend of *DGPI* can be approximated as:

$$\frac{\Delta DGPI}{\Delta t} \approx \left(\overline{U_y \times \omega \times \zeta_a} \times \frac{\Delta V_s}{\Delta t} + \overline{V_s \times \omega \times \zeta_a} \times \frac{\Delta U_y}{\Delta t} + \overline{V_s \times U_y \times \zeta_a} \times \frac{\Delta \omega}{\Delta t} + \overline{V_s \times U_y \times \omega} \times \frac{\Delta \zeta_a}{\Delta t}\right) e^{-11.8} \qquad (5)$$

On the right-hand-side of Eq. (5), the first term indicates the contribution of changes in vertical wind shear to that in *MPI*, the second term indicates the contribution of changes in 500-hPa zonal wind, the third term indicates the contribution of changes in mid-tropospheric vertical motion, and the last term indicates the contribution of changes in low-level vorticity.

Maximum potential intensity (MPI)

A TC can be considered as a Carnot engine, with its MPI primarily determined by its background environment, namely the thermodynamic efficiency and thermodynamic disequilibrium. Based on previous studies [47,48,56,57], the mathematical expression of a TC's *MPI* (unit: m/s) can be written as:

$$MPI = \sqrt{\frac{C_k}{C_D} \frac{T_S - T_0}{T_0} (h_0^* - h^*)} \qquad (6)$$

where C_k is the surface enthalpy exchange coefficient, C_D is the drag coefficient, T_S is the sea surface temperature (SST), T_0 is the outflow temperature of the TC, h_0^* is the saturation moist static energy (MSE) at the sea surface, and h^* is the saturation MSE of the free troposphere.

In Eq. (6), $\frac{C_k}{C_D}$ is usually taken as a constant, and is set as 0.9 in this study following Gilford[57]. The term $\frac{T_S - T_0}{T_0}$ indicates the thermodynamic efficiency (η), which increases as the temperature

gradient between the sea surface and upper troposphere deepens. The $h_0^* - h^*$ term is referred to as the thermodynamic disequilibrium (*L*) between the ocean and atmosphere, which determines the amount of energy that can be converted to TC's kinetic energy through convective heating. Larger magnitudes of *L* and η indicate that more energy can be potentially converted to a TC's kinetic energy from the surrounding environment. Following previous studies [48,57,58], $h_0^* - h^*$ is calculated as a residual from Eq. (6). All MPI calculations in this study are carried out using the pyPI (v1.3) Python package[57].

In order to quantify the contributions of changes in η and *L* to that in *MPI*, we again apply the product rule to the first derivative of Eq. (6).

$$\frac{\Delta MPI}{\Delta t} \approx \frac{1}{2\,\overline{MPI}} \frac{C_k}{C_D} \left(\bar{L}\frac{\Delta \eta}{\Delta t} + \bar{\eta}\frac{\Delta L}{\Delta t}\right) \quad (7)$$

where $\frac{\Delta MPI}{\Delta t}$, $\frac{\Delta \eta}{\Delta t}$, and $\frac{\Delta L}{\Delta t}$ denote the long-term linear trends of *MPI*, η, and *L*, respectively. $\overline{MPI}$, $\bar{\eta}$, and $\bar{L}$ denote the climatological average of *MPI*, η, and *L*, respectively. On the right-hand side of Eq. (7), the first term $\frac{1}{2\,\overline{MPI}} \frac{C_k}{C_D} \left(\bar{L}\frac{\Delta \eta}{\Delta t}\right)$ indicates the contribution of changes in η to that in *MPI*. Similarly, the second term $\frac{1}{2\,\overline{MPI}} \frac{C_k}{C_D} \left(\bar{\eta}\frac{\Delta L}{\Delta t}\right)$ indicates the contribution of changes in *L*.

In Fig. 4, we also explicitly derive the variation of MPI resulting solely from changes in L (MPI_L, Eq. 8) and η (MPI_η, Eq. 9), respectively.

$$MPI_L = \sqrt{\frac{C_k}{C_D} L\bar{\eta}} = \sqrt{\frac{C_k}{C_D} \frac{T_S - T_0}{T_0} \overline{(h_0^* - h^*)}} \quad (8)$$

$$MPI_\eta = \sqrt{\frac{C_k}{C_D} \bar{L}\eta} = \sqrt{\frac{C_k}{C_D} \left(\overline{\frac{T_S - T_0}{T_0}}\right) (h_0^* - h^*)} \quad (9)$$

Trend analysis and significance test

All trend values were calculated using linear regression. The statistical significance of all linear trends presented in the analyses was tested by the Mann-Kendall test. The Student's *t*-test was also employed and yielded the same conclusions as those by the Mann-Kendall test. All trend values presented in the main context are statistically significant at a confidence level of at least 90%, unless otherwise specified.

Data availability

The IBTrACS dataset is accessible through https://www.ncei.noaa.gov/products/international-best-track-archive. The NCEP2 reanalysis is accessible through https://www.psl.noaa.gov/data/gridded/data.ncep.reanalysis2.html. The OISSTv2 dataset is accessible through https://www.psl.noaa.gov/data/gridded/data.noaa.oisst.v2.highres.html.

Code availability

The Python package for MPI calculations is available at https://github.com/dgilford/tcpyPI/releases/tag/v1.3. Other codes employed in this article are available from the corresponding author on reasonable request.

Acknowledgments

The authors would like to thank Prof. Weihong Qian from Peking University for his valuable comments. This study was supported by the Independent Innovation Science Fund of National University of Defense Technology (22-ZZCX-081), the NUDT Research Initiation Funding for High-Level Scientific and Technological Innovative Talents (202402-YJRC-LJ-001), the Guangdong Province Introduction of Innovative R&D Team Project China (2019ZT08G669), the National Natural Science Foundation of China (42405038).

Competing interests

The authors declare no competing interests.

Author contributions

J.L: formal analysis, visualization, writing—original draft, writing—review and editing; J.C.H.L.: methodology, formal analysis, writing—original draft, writing—review and editing, funding acquisition; D.Z., D.X., H.H., Z.Z.: writing—review and editing; W.T., Y.M., Y.L.: supervision, writing—review and editing, funding acquisition; B.Z.: conceptualization, supervision, methodology, writing—original draft, writing—review and editing, funding acquisition.

References

1. Walsh, K. J. E. *et al.* Tropical cyclones and climate change. *WIREs Climate Change* **7**, 65–89 (2016).
2. Klotzbach, P. J. *et al.* Surface Pressure a More Skillful Predictor of Normalized Hurricane Damage than Maximum Sustained Wind. *Bull Am Meteorol Soc* **101**, E830–E846 (2020).
3. Zhang, X. *et al.* Spatial pattern of the population casualty rate caused by super typhoon Lekima and quantification of the interactive effects of potential impact factors. *BMC Public Health* **21**, 1260 (2021).
4. In pictures: Record-breaking Hurricane Beryl. *CNN*

https://www.cnn.com/2024/07/02/weather/gallery/hurricane-beryl (2024).
5. Tropical cyclone Chido devastates Mayotte in Indian Ocean. *World Meteorological Organization* https://wmo.int/media/news/tropical-cyclone-chido-devastates-mayotte-indian-ocean (2024).
6. Knutson, T. R. *et al.* Tropical cyclones and climate change. *Nat Geosci* **3**, 157–163 (2010).
7. Elsner, J. B., Kossin, J. P. & Jagger, T. H. The increasing intensity of the strongest tropical cyclones. *Nature* **455**, 92–95 (2008).
8. Wang, J. *et al.* Changing Lengths of the Four Seasons by Global Warming. *Geophys Res Lett* **48**, e2020GL091753 (2021).
9. Huang, P., Xie, S.-P., Hu, K., Huang, G. & Huang, R. Patterns of the seasonal response of tropical rainfall to global warming. *Nat Geosci* **6**, 357–361 (2013).
10. Geng, Y.-F., Xie, S.-P., Zheng, X.-T. & Wang, C.-Y. Seasonal Dependency of Tropical Precipitation Change under Global Warming. *J Clim* **33**, 7897–7908 (2020).
11. Gan, Q., Leung, J. C.-H., Wang, L. & Zhang, B. Weakening seasonality of Indo-Pacific warm pool size in a warming world since 1950. *Environmental Research Letters* **18**, 14024 (2023).
12. Shi, J.-R., Santer, B. D., Kwon, Y.-O. & Wijffels, S. E. The emerging human influence on the seasonal cycle of sea surface temperature. *Nat Clim Chang* **14**, 364–372 (2024).
13. Liu, F., Song, F. & Luo, Y. Human-induced intensified seasonal cycle of sea surface temperature. *Nat Commun* **15**, 3948 (2024).
14. Hänninen, H. & Tanino, K. Tree seasonality in a warming climate. *Trends Plant Sci* **16**, 412–416 (2011).
15. Wang, H. *et al.* Anthropogenic climate change has influenced global river flow seasonality. *Science (1979)* **383**, 1009–1014 (2024).
16. Hahn, L. C., Armour, K. C., Battisti, D. S., Eisenman, I. & Bitz, C. M. Seasonality in Arctic Warming Driven by Sea Ice Effective Heat Capacity. *J Clim* **35**, 1629–1642 (2022).
17. Loo, Y. Y., Billa, L. & Singh, A. Effect of climate change on seasonal monsoon in Asia and its impact on the variability of monsoon rainfall in Southeast Asia. *Geoscience Frontiers* **6**, 817–823 (2015).
18. Moustakis, Y., Papalexiou, S. M., Onof, C. J. & Paschalis, A. Seasonality, Intensity, and Duration of Rainfall Extremes Change in a Warmer Climate. *Earths Future* **9**, e2020EF001824 (2021).
19. Lopez, H. *et al.* Projected increase in the frequency of extremely active Atlantic hurricane seasons. *Sci Adv* **10**, eadq7856 (2024).
20. Kossin, J. P. Is the North Atlantic hurricane season getting longer? *Geophys Res Lett* **35**, (2008).
21. Zuo, H., Li, T., Liu, J. & Peng, M. What controls early or late onset of tropical North Atlantic hurricane season? *Journal of Meteorological Research* **30**, 298–311 (2016).
22. Truchelut, R. E. *et al.* Earlier onset of North Atlantic hurricane season with warming oceans. *Nat Commun* **13**, 4646 (2022).
23. Huang, H. *et al.* Recent Unusual Consecutive Spring Tropical Cyclones in North Atlantic and Winter Oceanic Precursor Signals. *Journal of Meteorological Research* **37**, 208–217 (2023).
24. Keim, B. D. & Robbins, K. D. Occurrence dates of North Atlantic tropical storms and hurricanes: 2005 in perspective. *Geophys Res Lett* **33**, (2006).
25. Zhang, G. Warming-induced contraction of tropical convection delays and reduces tropical

cyclone formation. *Nat Commun* **14**, 6274 (2023).
26. Karloski, J. M. & Evans, C. Seasonal Influences upon and Long-Term Trends in the Length of the Atlantic Hurricane Season. *J Clim* **29**, 273–292 (2015).
27. Dwyer, J. G. *et al.* Projected Twenty-First-Century Changes in the Length of the Tropical Cyclone Season. *J Clim* **28**, 6181–6192 (2015).
28. Patricola, C. M., Hansen, G. E. & Sena, A. C. T. The Influence of Climate Variability and Future Climate Change on Atlantic Hurricane Season Length. *Geophys Res Lett* **51**, e2023GL107881 (2024).
29. Kossin, J. P., Knapp, K. R., Olander, T. L. & Velden, C. S. Global increase in major tropical cyclone exceedance probability over the past four decades. *Proceedings of the National Academy of Sciences* **117**, 11975–11980 (2020).
30. Lee, C.-Y., Tippett, M. K., Sobel, A. H. & Camargo, S. J. Rapid intensification and the bimodal distribution of tropical cyclone intensity. *Nat Commun* **7**, 10625 (2016).
31. Bhatia, K. *et al.* A potential explanation for the global increase in tropical cyclone rapid intensification. *Nat Commun* **13**, 6626 (2022).
32. Patricola, C. M. & Wehner, M. F. Anthropogenic influences on major tropical cyclone events. *Nature* **563**, 339–346 (2018).
33. Mei, W., Xie, S.-P., Primeau, F., McWilliams, J. C. & Pasquero, C. Northwestern Pacific typhoon intensity controlled by changes in ocean temperatures. *Sci Adv* **1**, e1500014 (2025).
34. Li, Y. *et al.* Recent increases in tropical cyclone rapid intensification events in global offshore regions. *Nat Commun* **14**, 5167 (2023).
35. Bloemendaal, N. *et al.* A globally consistent local-scale assessment of future tropical cyclone risk. *Sci Adv* **8**, eabm8438 (2025).
36. Chih, C.-H. *et al.* Intense Tropical Cyclones in the Western North Pacific Under Global Warming: A Dynamical Downscaling Approach. *Journal of Geophysical Research: Atmospheres* **129**, e2023JD038598 (2024).
37. Shan, K., Lin, Y., Chu, P.-S., Yu, X. & Song, F. Seasonal advance of intense tropical cyclones in a warming climate. *Nature* **623**, 83–89 (2023).
38. Wu, Y., Huang, F. & Xu, S. The earlier end of the tropical cyclone season over the Western North Pacific by environmental cyclogenesis factors. *Clim Dyn* **61**, 1293–1309 (2023).
39. Hsu, P.-C., Chu, P.-S., Murakami, H. & Zhao, X. An Abrupt Decrease in the Late-Season Typhoon Activity over the Western North Pacific. *J Clim* **27**, 4296–4312 (2014).
40. Wang, B. & Murakami, H. Dynamic genesis potential index for diagnosing present-day and future global tropical cyclone genesis. *Environmental Research Letters* **15**, 114008 (2020).
41. Murakami, H. & Wang, B. Patterns and frequency of projected future tropical cyclone genesis are governed by dynamic effects. *Commun Earth Environ* **3**, 77 (2022).
42. Wu, Y. & Korty, R. L. Changes in the Length of the Season with Favorable Environmental Conditions for Tropical Cyclones in the North Atlantic Basin during the Last 40 Years. *J Clim* **35**, 5237–5256 (2022).
43. L'Heureux, M. L., Lee, S. & Lyon, B. Recent multidecadal strengthening of the Walker circulation across the tropical Pacific. *Nat Clim Chang* **3**, 571–576 (2013).
44. Kang, S. M. *et al.* Walker circulation response to extratropical radiative forcing. *Sci Adv* **6**, eabd3021 (2024).
45. Zhang, W. *et al.* Dominant Role of Atlantic Multidecadal Oscillation in the Recent Decadal

Changes in Western North Pacific Tropical Cyclone Activity. *Geophys Res Lett* **45**, 354–362 (2018).
46. Gilford, D. M., Solomon, S. & Emanuel, K. A. On the Seasonal Cycles of Tropical Cyclone Potential Intensity. *J Clim* **30**, 6085–6096 (2017).
47. Emanuel, K. A. The dependence of hurricane intensity on climate. *Nature* **326**, 483–485 (1987).
48. Wing, A. A., Emanuel, K. & Solomon, S. On the factors affecting trends and variability in tropical cyclone potential intensity. *Geophys Res Lett* **42**, 8669–8677 (2015).
49. Matthews, T., Wilby, R. L. & Murphy, C. An emerging tropical cyclone–deadly heat compound hazard. *Nat Clim Chang* **9**, 602–606 (2019).
50. Gori, A., Lin, N. & Xi, D. Tropical Cyclone Compound Flood Hazard Assessment: From Investigating Drivers to Quantifying Extreme Water Levels. *Earths Future* **8**, e2020EF001660 (2020).
51. Knapp, K. R., Kruk, M. C., Levinson, D. H., Diamond, H. J. & Neumann, C. J. The international best track archive for climate stewardship (IBTrACS). *Bull Am Meteorol Soc* **91**, 363–376 (2010).
52. Liu, J. *et al.* Questioning whether seasonal advance of intense tropical cyclones since the 1980s truly exists. *Preprint at https://arxiv.org/abs/2403.00330* (2024).
53. Huang, B. *et al.* Improvements of the Daily Optimum Interpolation Sea Surface Temperature (DOISST) Version 2.1. *J Clim* **34**, 2923–2939 (2021).
54. Kanamitsu, M. *et al.* NCEP–DOE AMIP-II Reanalysis (R-2). *Bull Am Meteorol Soc* **83**, 1631–1644 (2002).
55. Huang, H. *et al.* Recent Unusual Consecutive Spring Tropical Cyclones in North Atlantic and Winter Oceanic Precursor Signals. *Journal of Meteorological Research* **37**, 208–217 (2023).
56. Emanuel, K. A. An Air-Sea Interaction Theory for Tropical Cyclones. Part I: Steady-State Maintenance. *Journal of Atmospheric Sciences* **43**, 585–605 (1986).
57. Gilford, D. M. pyPI (v1.3): Tropical Cyclone Potential Intensity Calculations in Python. *Geosci Model Dev* **14**, 2351–2369 (2021).
58. Shields, S., Wing, A. A. & Gilford, D. M. A Global Analysis of Interannual Variability in Potential and Actual Tropical Cyclone Intensities. *Geophys Res Lett* **47**, e2020GL089512 (2020).

Supplementary Files

This is a list of supplementary files associated with this preprint. Click to download.

- suppintensetcseason20250114.docx